Article

Isoquinoline Alkaloids as Protein Tyrosine Phosphatase Inhibitors from a Deep-Sea-Derived Fungus *Aspergillus puniceus*

Cheng-Mei Liu [1,2], Fei-Hua Yao [1,2], Xin-Hua Lu [4], Xue-Xia Zhang [4], Lian-Xiang Luo [5], Xiao Liang [1] and Shu-Hua Qi [1,3,*]

1   CAS Key Laboratory of Tropical Marine Bio-Resources and Ecology, Guangdong Key Laboratory of Marine Materia Medica, Innovation Academy of South China Sea Ecology and Environmental Engineering, South China Sea Institute of Oceanology, Chinese Academy of Sciences, Guangzhou 510301, China; liuchengmei19@mails.ucas.ac.cn (C.-M.L.); yaofeihua20@malls.ucas.ac.cn (F.-H.Y.); liangxiao@scsio.ac.cn (X.L.)
2   University of Chinese Academy of Sciences, Beijing 100049, China
3   Southern Marine Science and Engineering Guangdong Laboratory, 1119 Haibin Road, Guangzhou 511458, China
4   New Drug Research & Development Co., Ltd., North China Pharmaceutical Group Corporation, Shijiazhuang 050015, China; luxinhua89@hotmail.com (X.-H.L.); zhangxuexiazxx@163.com (X.-X.Z.)
5   The Marine Biomedical Research Institute, Guangdong Medical University, Zhanjiang 524023, China; luolianxiang321@gdmu.edu.cn
*   Correspondence: shuhuaqi@scsio.ac.cn; Tel.: +86-208-9022-112; Fax: +86-208-4458-964

Abstract: Puniceusines A–N (**1–14**), 14 new isoquinoline alkaloids, were isolated from the extracts of a deep-sea-derived fungus, *Aspergillus puniceus* SCSIO z021. Their structures were elucidated by spectroscopic analyses. The absolute configuration of **9** was determined by ECD calculations, and the structures of **6** and **12** were further confirmed by a single-crystal X-ray diffraction analysis. Compounds **3–5** and **8–13** unprecedentedly contained an isoquinolinyl, a polysubstituted benzyl or a pyronyl at position C-7 of isoquinoline nucleus. Compounds **3** and **4** showed selective inhibitory activity against protein tyrosine phosphatase CD45 with IC_{50} values of 8.4 and 5.6 µM, respectively, **4** also had a moderate cytotoxicity towards human lung adenocarcinoma cell line H1975 with an IC_{50} value of 11.0 µM, and **14**, which contained an active center, -C=N$^+$, exhibited antibacterial activity. An analysis of the relationship between the structures, enzyme inhibitory activity and cytotoxicity of **1–14** revealed that the substituents at C-7 of the isoquinoline nucleus could greatly affect their bioactivity.

Keywords: deep-sea-derived fungus; *Aspergillus puniceus*; isoquinoline alkaloid; protein tyrosine phosphatase inhibitor; cytotoxicity; antibacterial

1. Introduction

Isoquinoline alkaloids are a large group of alkaloids in the plant kingdom, showing diverse pharmacological and biological activities such as anticancer, anti-inflammatory, cholesterol-lowering, antihyperglycemic, antiplasmodial, antifungal, and antimicrobial activity, etc. [1]. According to their structural components, isoquinoline and tetrahydroisoquinoline alkaloids can be classified into over 20 sub-classes, mainly including simple isoquinoline, benzylisoquinoline, bisbenzylisoquinoline, proto-berberine alkaloid, and aporphine alkaloid, etc. [1]. The most famous representative of this group is antidiabetic berberine. However, only a few isoquinoline alkaloids have been isolated from fungi, such as TMC-120A, B and C from *Aspergillus ustus* [2] and *A. insuetus* [3]; chaetoindicins A–C from *Chaetomium indicum* [4]; fusarimine from *Fusarium* sp. [5]; 8-methoxy-3,5-dimethylisoquinolin-6-ol from *Penicillium citrinum* [6]; azaphilone from *P. sclerotiorum* [7]; and spathullins A–B from *P. spathulatum* [8].

Malfunctions in protein tyrosine phosphatase (PTP) activity are linked to various diseases, ranging from cancer to neurological disorders and diabetes, such as CD45, SHP1, TCPTP, PTP1B and LAR linked to cancer, CD45, SHP1 and LAR also linked to neurological diseases, and PTP1B and LAR also linked to diabetes, etc. [9]. Some PTPs emerged as promising targets for therapeutic intervention in recent years [9,10]. However, achieving the selectivity of PTP inhibitors is a big challenge. In recent years, we obtained a series of natural compounds including anthraquinones [11], meroterpenoids [12], xanthone-type and anthraquinone-type mycotoxins [13], and oxaphenalenones [14] as PTP inhibitors from marine-derived fungi. In order to further explore diversified bioactive compounds from the deep-sea-derived fungus, *Aspergillus puniceus* SCSIO z021, we changed culture media and further conducted a chemical investigation of this strain cultured with a complex medium, which led to the characterization of 14 undescribed isoquinoline alkaloids, puniceusines A–N (**1**–**14**) (Figure 1). Compounds **1**–**14** were evaluated for their enzyme inhibitory activity against five kinds of PTPs, cytotoxicity towards human lung adenocarcinoma cell line H1975, and antibacterial activity. Herein, we report the isolation, structure elucidation and bioactivities of **1**–**14**.
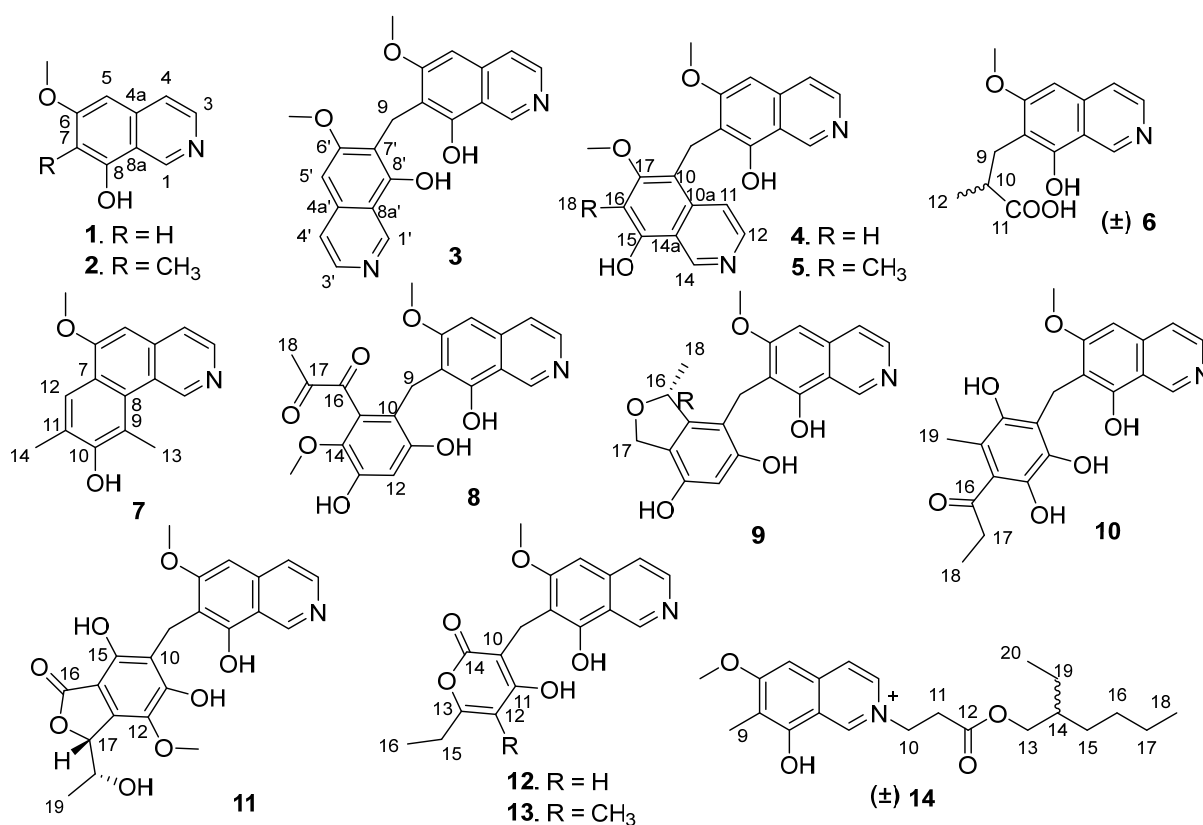

Figure 1. Structures of the isolated compounds **1**–**14**.

2. Results and Discussion

Puniceusine A (**1**) has the molecular formula $C_{10}H_9NO_2$, as determined by HRESIMS. The ^{1}H NMR spectrum (Table 1) showed the presence of one methoxy group at δ_H 3.96 (3H, s) and five aromatic hydrogens at δ_H 9.45 (1H, s), 8.40 (1H, d, *J* = 5.7 Hz), 8.06 (1H, d, *J* = 6.4 Hz), 7.13 (1H, s), 6.81 (1H, s). The ^{13}C NMR spectrum (Table 2) showed 10 carbon signals including one methoxy, five aromatic methines, and four aromatic non-protonated carbons. These NMR data were similar to those of 6,8-dimethoxyisoquinolin [15] and papraline [16], and the only clear difference between **1** and 6,8-dimethoxyisoquinolin was the disappearance of one oxygenated methyl, which indicated that **1** was also an isoquinoline alkaloid. This was supported by the HMBC spectrum showing correlations

from H-1 to C-3/C-4a/C-8a, H-3 to C-4/C-4a, H-4 to C-3/C-5/C-8a, H-5 to C-4/C-6/C-7/C-8a, and H-7 to C-5/C-6/C-8/C-8a. In addition, the HMBC correlation from δ_H 3.96 (3H, s) to C-6 suggested that a methoxy group was attached at C-6. Thus, the structure of **1** was determined to be 6-methoxy-8-hydroxy-isoquinolin.

Table 1. ^{1}H NMR Data for Compounds **1–7** (δ in ppm, *J* in Hz) in DMSO-d_6 or Methanol-d_4.

No.	1 [a,c]	2 [a,d]	3 [b,d]	4 [a,d]	5 [a,d]	6 [a,d]	7 [b,d]
1	9.45, s	9.41, s	9.34, s	9.59, s	9.58, s	9.49, s	9.87, s
3	8.40, d (5.7)	8.24 d (6.5)	8.08, d (6.3)	8.29, d (7.0)	8.30, d (6.6)	8.29, d (6.0)	8.47, d (6.3)
4	8.06, d (6.4)	8.04 d (6.5)	7.90, d (6.3)	8.05, d (6.5)	8.09, d (6.6)	8.10, d (6.0)	8.22, d (6.3)
5	7.13, s	7.13 s	6.95, s	7.11, s	7.18, s	7.23, s	7.31, s
7	6.81, s						
9		2.25, s	4.32, s	4.47, s	4.61, s	2.97, dd (14.0, 5.5) 3.17, dd (14.0, 8.5)	
10						2.85, m	
11				8.58, d (7.0)	8.67, d (6.8)		
12				8.31, d (7.8)	8.39, d (6.8)	1.27, d (7.5)	8.24, s
13							2.93, s
14				9.52, s	9.68, s		2.51, s
16				7.00, s			
18					2.38, s		
6-OCH$_3$	3.96, s	4.07, s	4.09, s	3.79, s	3.84, s	4.10, s	4.24, s
6′-OCH$_3$			4.09, s				
17-OCH$_3$				3.98, s	3.79, s		

[a] 500 MHz for ^{1}H NMR; [b] 700 MHz for ^{1}H NMR; [c] DMSO-d_6; [d] Methanol-d_4.

Table 2. ^{13}C NMR data for Compounds **1–8** (δ in ppm) in DMSO-d_6 or Methanol-d_4.

No.	1 [a,c]	2 [a,d]	3 [b,d]	4 [a,d]	5 [a,d]	6 [a,d]	7 [b,d]	8 [a,c]
1	141.8, CH	141.5, CH	141.9, CH	142.4, CH	142.3, CH	142.3, CH	132.7, CH	141.2, CH
3	133.2, CH	131.4, CH	130.8, CH	132.1, CH	132.0, CH	132.2, CH	123.5, CH	131.5, CH
4	122.3, CH	123.7, CH	123.1, CH	123.7, CH	123.9, CH	123.8, CH	114.7, CH	122.0, CH
4a	140.9, C	140.9, C	141.2, C	141.5, C	141.5, C	141.6, C	137.2, C	139.1, C
5	97.8, CH	98.6, CH	96.1, C	98.8, CH	99.4, CH	99.0, CH	90.3, CH	97.2, CH
6	166.9, C	168.4, C	169.1, C	168.5, C	168.2, C	168.3, C	155.0, C	165.8, C
7	103.5, CH	116.8, C	118.9, C	118.5, C	120.8, C	119.1, C	113.3, C	117.3, C
8	158.6, C	155.7, C	163.9, C	156.3, C	156.2, C	156.4, C	121.2, C	155.8, C
8a	115.5, C	117.5, C	118.7, C	117.8, C	117.9, C	117.9, C	114.0, C	115.8, C
9		9.2, CH$_3$	19.4, CH$_2$	20.7, CH$_2$	21.3, CH$_2$	28.0, CH$_2$	112.0, C	19.3, CH$_2$
10				113.6, C	120.0, C	40.4, CH	148.7, C	115.0, C
10a				139.7, C	138.9, C			
11				121.6, CH	122.7, CH	181.7, C	120.7, C	151.3, C
12				131.2, CH	131.0, CH	18.1, CH$_3$	115.0, C	107.1, CH
13							8.0, CH$_3$	139.5, C
14				143.3, CH	143.4, CH		8.4, CH$_3$	148.1, C
14a				115.9, C	119.0, C			
15				161.0, C	156.7, C			130.2, C
16				100.1, CH	120.6, C			195.1, C
17				167.5, C	167.7, C			196.9, C
18					10.8, CH$_3$			23.7, CH$_3$
6-OCH$_3$	56.4, CH$_3$	57.4, CH$_3$	57.0, CH$_3$	56.9, CH$_3$	57.0, CH$_3$	57.4, CH$_3$	47.9, CH$_3$	56.4, CH$_3$
14-OCH$_3$								59.7, CH$_3$
17-OCH$_3$				57.1, CH$_3$	62.1, CH$_3$			

[a] 125 MHz for ^{13}C NMR; [b] 175 MHz for ^{13}C NMR; [c] DMSO-d_6; [d] Methanol-d_4.

Puniceusine B (**2**) was assigned the molecular formula $C_{11}H_{11}NO_2$ by HRESIMS. The ^{1}H NMR and ^{13}C NMR data (Tables 1 and 2) showed great similarity to those of **1**, and the main difference between them was the additional presence of one methyl (δ_H 2.25, 3H, s; δ_C 9.2) and the disappearance of one aromatic hydrogen in **2**. The HMBC correlations from δ_H 2.25 to C-6/C-7/C-8 suggested the additional methyl attached at C-7. Hence, the structure of **2** was determined to be 6-methoxy-7-methyl-8-hydroxy-isoquinolin.

Puniceusine C (**3**) was found to have the molecular formula $C_{21}H_{18}N_2O_4$ by HRESIMS that was nearly twice that of **2**. The ^{1}H and ^{13}C NMR data (Tables 1 and 2) showed great similarity to those of **2**, and the clearest difference between them was the disappearance of a methyl signal and the additional presence of a methylene signal (δ_H 4.32, 2H, s; δ_C 19.4) in **3**. The ^{1}H NMR spectrum of **3** showed a double increase in the integral areas for H-1, H-3, H-4, H-5, and a methoxy group. The HMBC correlations (Figure 2) from δ_H 4.32 (H$_2$-9) to C-6/C-7/C-8 suggested a methylene instead of a methyl attached at C-7. These data indicated that **3** was a symmetrical dimer of **1**, connected at positions C-7′ and C-7 by a methylene C-9. Thus, the structure of **3** was determined as shown.
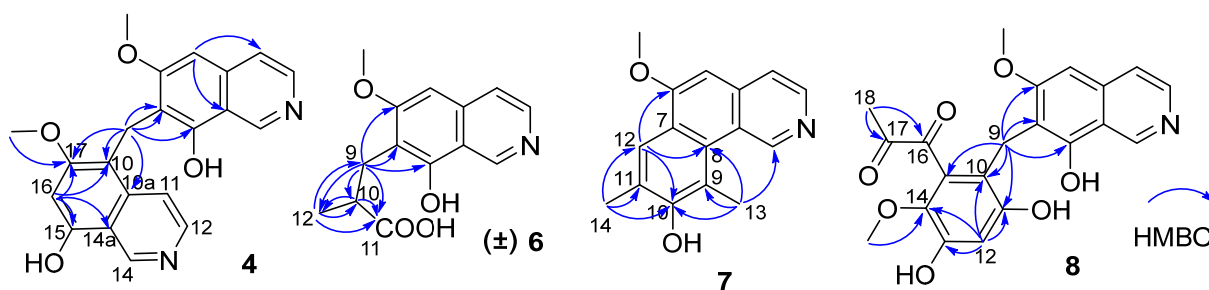

Figure 2. Key HMBC correlations of compounds **4**, **6–8**.

Puniceusine D (**4**) showed the same molecular formula of $C_{21}H_{18}N_2O_4$ as that of **3** by analysis of its HRESIMS and NMR data (Tables 1 and 2). The ^{1}H NMR spectrum showed the presence of two downfield hydrogens at δ_H 9.59 (1H, s) and 9.52 (1H, s); six aromatic hydrogens at δ_H 8.58 (1H, d, *J* = 7.0 Hz), 8.31 (1H, d, *J* = 7.8 Hz), 8.29 (1H, d, *J* = 7.0 Hz), 8.05 (1H, d, *J* = 6.5 Hz), 7.11 (1H, s), and 7.00 (1H, s); two methoxys groups at δ_H 3.79 (3H, s) and 3.98 (3H, s); and one methylene at δ_H 4.47 (2H, s). The ^{13}C NMR spectrum showed 21 carbon signals including one methylene, two methoxyls, eight aromatic methines, and ten aromatic non-protonated carbons. These data showed similarity to those of **1–3**, which indicated that **4** was also a dimer of **1**. The HMBC correlations from H-5 to C-4/C-8a, from H-16 to C-10/C-14a/C-15/C-17, and from H$_2$-9 to C-6/C-7/C-8/C-10/C-10a/C-17 (Figure 2) suggested that **4** was an asymmetric dimer of **1** connected at positions C-7 and C-10 by a methylene C-9. The two methoxy groups were attached at C-6 and C-17 based on the HMBC correlations of δ_H 3.98 (3H, s) with C-17 and δ_H 3.79 (3H, s) with C-6, respectively. Therefore, the structure of **4** was established as shown.

The molecular formula of puniceusine E (**5**) was determined as $C_{22}H_{21}N_2O_4$ by HRES-IMS. The ^{1}H and ^{13}C NMR data (Tables 1 and 2) of **5** were greatly similar to those of **4**, and the only obvious difference between them was the absence of one aromatic hydrogen and the additional presence of one methyl signal (δ_H 2.38, 3H, s; δ_C 10.8) in **5**. The HMBC correlations from H$_3$-18 (δ_H 2.38) to C-15/C-16/C-17 suggested a methyl located at C-16 instead of a hydrogen. Thus, the structure of **5** was established as shown.

Puniceusine F (**6**) had the molecular formula $C_{14}H_{15}NO_4$, as determined by HRES-IMS. The ^{1}H and ^{13}C NMR data (Tables 1 and 2) of **6** were similar to those of **1**, and the clearest difference between them was the disappearance of one aromatic hydrogen and the additional presence of one methyl (δ_H 1.27, d, *J* = 7.5 Hz, 3H), one methylene, one methine, and one carboxyl group in **6**. The HMBC correlations (Figure 2) from H$_2$-9 (δ_H 2.97 (dd, *J* = 14.0, 5.5 Hz, 1H), 3.17 (dd, *J* = 14.0, 8.5 Hz, 1H)) to C-6/C-7/C-8/C-10/C-11/C-12, from H-10 (δ_H 2.85, m, 1H) to C-11/C-12, and from H$_3$-12 (δ_H 1.27, d, *J* =7.5 Hz, 3H) to C-9/C-10/C-11 suggested an isobutyric acid group attached at C-7 of the isoquinoline

nucleus. The optical rotation and measured CD data of **6** were zero, which indicated that **6** was a racemic mixture. This was supported by the HPLC analysis of **6** with a chiral column (CHIRALPAK IA 4.6 mm × 250 mm column) eluting with n-hexane/ethanol/TFA (68:32:0.2, *v/v*) (Figure S39). This structure was further confirmed by a single-crystal X-ray diffraction analysis (Figure 3).
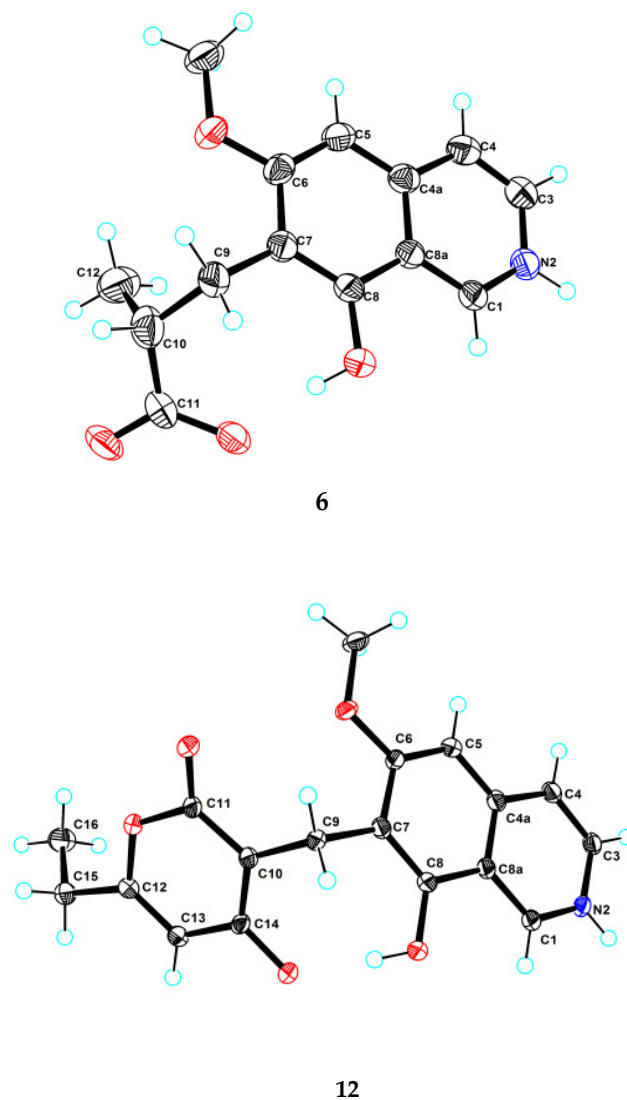

6

12

Figure 3. Ortep plot of the X-ray crystallographic data for **6** and **12**.

The molecular formula of puniceusine G (**7**) was determined to be $C_{16}H_{15}NO_2$, according to its HRESIMS. The ^1H and ^{13}C NMR data (Tables 1 and 2) of **7** were similar to those of **1**, and the clearest difference between them was the additional presence of two double bonds (δ_C 112.0 (C, C-9), 115.0 (CH, C-12), 120.7 (C, C-11), 148.7 (C, C-10)) and two methyls (δ_H 2.51 (3H, s, H-14), 2.93 (3H, s, H-13); δ_C 8.0, 8.4) in **7**. The HMBC correlations (Figure 2) from H-12 to C-6/C-8/C-10, from H_3-13 to C-1/C-8/C-9/C-10, and from H_3-14 to C-10/C-11/C-12, suggested a 3,5-dimethyl-4-hydroxyphenyl group attached at the isoquinoline nucleus by sharing C-7 and C-8 to form a benzo[*h*]isoquinoline unit. Therefore, the structure of **7** was established as shown.

Puniceusine H (**8**) had the molecular formula of $C_{21}H_{19}NO_7$ as determined by its HRESIMS. The ^1H and ^{13}C NMR data (Tables 2 and 3) of **8** showed similarity to those of **4–6** with the presence of characteristic chemical shifts for a methylene C-9 (δ_H 4.01 (2H, s), δ_C 19.3 (CH_2)). The HMBC correlations (Figure 2) from H_2-9 to C-6/C-7/C-8/C-10/C-11/C-15, from H-12 (δ_H 6.58, 1H, s) to C-10/C-11/C-13/C-14, and from H_3-19 (δ_H 3.52, 3H, s) to C-14 suggested a 2,4-dihydroxy-5-methoxyphenyl fragment connected with isoquinoline unit by a methylene at position C-7. In addition, the HMBC correlations from H_3-18 (δ_H 2.30, 3H, s) to C-16 (δ_C 195.1, C)/C-17 (δ_C 196.9, C) suggested the presence of a 1,2-propanedione group that was exclusively assigned to attach at C-15 of the benzene ring based on the above data. Thus, the structure of **8** was established as shown.

Table 3. ^1H NMR data for Compounds **8–14** (δ in ppm, *J* in Hz) in DMSO-d_6 or Methanol-d_4.

| No.	8 [a,c]	9 [b,c]	10 [b,d]	11 [a,d]	12 [a,d]	13 [a,d]	14 [a,d]
1	9.49, s	9.51, s	9.47, s	9.49, s	9.48, s	9.52, s	9.64, s
3	8.36, d (6.6)	8.39, d (6.6)	8.23, d (6.6)	8.25, d (6.4)	8.26, d (5.5)	8.29, d (6.6)	8.37, d (6.9)
4	8.08, d (6.6)	8.11, d (6.6)	8.05, d (6.6)	8.06, d (6.4)	8.06, d (5.5)	8.10, d (6.6)	8.08, d (6.9)
5	7.11, s	7.26, s	7.17, s	7.16, s	7.16, s	7.23, s	7.19, s
9	4.01, s	3.84, d (14.9) 4.03, d (14.8)	3.96, s	4.21, s	3.92, s	3.97, s	2.29, s
10							4.88, t (6.3)
11							3.18, t (6.3)
12	6.58, s	6.27, s			6.12, s		
13							4.00, d (5.7)
14							1.46, m
15					2.52, q (7.5)	2.60, q (7.5)	1.16, m
16		5.22, m			1.19, t (7.5)	1.17, t (7.5)	1.17, m
17		4.69, d (11.5) 4.84, dd (11.5, 2.5)	2.58, q (7.3)	5.56, d (2.5)		2.01, s	1.18, m
18	2.30, s	1.35, d (6.2)	1.02, t (7.3)	4.36, qd (6.5, 2.5)			0.79, t (7.5)
19	3.52, s		1.92, s	0.94, d (6.5)			1.24, m
20							0.82, t (6.5)
6-OCH₃	3.77, s	4.00, s	4.11, s	4.03, s	4.07, s	4.13, s	
12-OCH₃				3.76, s			

[a] 500 MHz for ^1H NMR; [b] 700 MHz for ^1H NMR; [c] DMSO-d_6; [d] Methanol-d_4.

Puniceusine I (**9**) had the molecular formula of $C_{20}H_{19}NO_5$ according to its HRESIMS with 12 degrees of unsaturation. The ^1H and ^{13}C NMR data (Tables 3 and 4) of **9** were similar to those of **8**, and the clearest difference between them was the disappearance of two keto carbons and one methoxy and the additional presence of one oxygenated methylene (δ_H 4.84 (1H, dd, *J* = 11.5, 2.5 Hz), 4.69 (1H, dd, *J* = 11.5 Hz), δ_C 68.9, CH_2) and one oxygenated methine (δ_H 5.22 (1H, m), δ_C 79.3, CH). A detailed analysis of HSQC and HMBC spectra proved that **9** also contained a 1,2,4,5,6-pentasubstituted-benzyl attached at C-7 of isoquinoline nucleus. In addition, the HMBC correlations from H-16 to C-14/C-15/C-17, from H_2-17 to C-10/C-11/C-12/C-13/C-14/C-15/C-16/C-18, from H_3-18 (δ_H 1.35, d, *J* = 6.2 Hz, 3H) to C-15/C-16 (Figure 4), suggested a 2-methyl-2,5-dihydrofuran ring connected with the benzene ring via C-14 and C-15. Therefore, the 2D structure of **9** was established as shown. The absolute configuration of **9** was further determined by electronic circular dichroism (ECD) calculations (Tables S1–S3).

Table 4. ^{13}C NMR data for Compounds **9–14** (δ in ppm) in DMSO-d_6 or Methanol-d_4.

No.	9 [b,c]	10 [b,d]	11 [a,d]	12 [a,d]	13 [a,d]	14 [a,d]
1	141.2, CH	142.3, CH	142.0, C	142.2, CH	142.4, CH	145.4, CH
3	131.5, CH	131.7, CH	131.6, CH	131.8, CH	132.0, CH	134.9, CH
4	122.2, CH	123.6, CH	123.6, CH	123.6, CH	123.9, CH	124.4, CH
4a	139.0, C	141.5, C	141.4, C	141.5, C	141.7, C	139.7, C
5	97.7, CH	98.4, C	98.7, CH	98.8, C	98.9, CH	98.6, CH
6	165.6, C	168.1, C	168.7, C	168.3, C	167.7, C	168.8, C
7	117.7, C	119.2, C	118.7, C	119.1, C	118.8, C	117.1, C
8	154.8, C	158.7, C	156.7, C	157.4, C	157.5, C	155.8, C
8a	115.5, C	118.4, C	117.6, C	118.0, C	118.3, C	117.7, C
9	19.8, CH$_2$	19.4, CH$_2$	18.9, CH$_2$	18.7, CH$_2$	19.3, CH$_2$	9.23, CH$_3$
10	109.4, C	101.5, C	116.2, C	101.0, C	100.9, C	57.1, CH$_2$
11	154.8, C	170.0, C	157.1, C	170.2, C	169.7, C	35.7, CH$_2$
12	101.4, CH	163.1, C	136.8, C	101.2, CH	109.8, C	171.8, C
13	150.1, C	113.8, C	137.4, C	167.4, C	162.7, C	68.4, CH$_2$
14	115.9, C	154.4, C	104.2, C	171.2, C	170.7, C	40.0, CH
15	145.3, C	171.6, C	153.0, C	27.4, CH$_2$	25.1, CH$_2$	31.3, CH$_2$
16	79.3, CH	207.3, C	172.7, C	11.2, CH$_3$	11.8, CH$_3$	29.9, CH$_2$
17	68.9, CH$_2$	36.6, CH$_2$	85.2, CH		9.9, CH$_3$	23.9, CH$_2$
18	21.3, CH$_3$	7.8, CH$_3$	68.6, CH			14.3, CH$_3$
19		10.4, CH$_3$	15.8, CH$_3$			24.6, CH$_2$
20						11.2, CH$_3$
6-OCH$_3$	56.7, CH$_3$	57.3, CH$_3$	57.2, CH$_3$	57.2, CH$_3$	57.5, CH$_3$	57.5, CH$_3$
12-OCH$_3$			61.1, CH$_3$			

[a] 125 MHz for ^{13}C NMR; [b] 175 MHz for ^{13}C NMR; [c] DMSO-d_6; [d] Methanol-d_4.
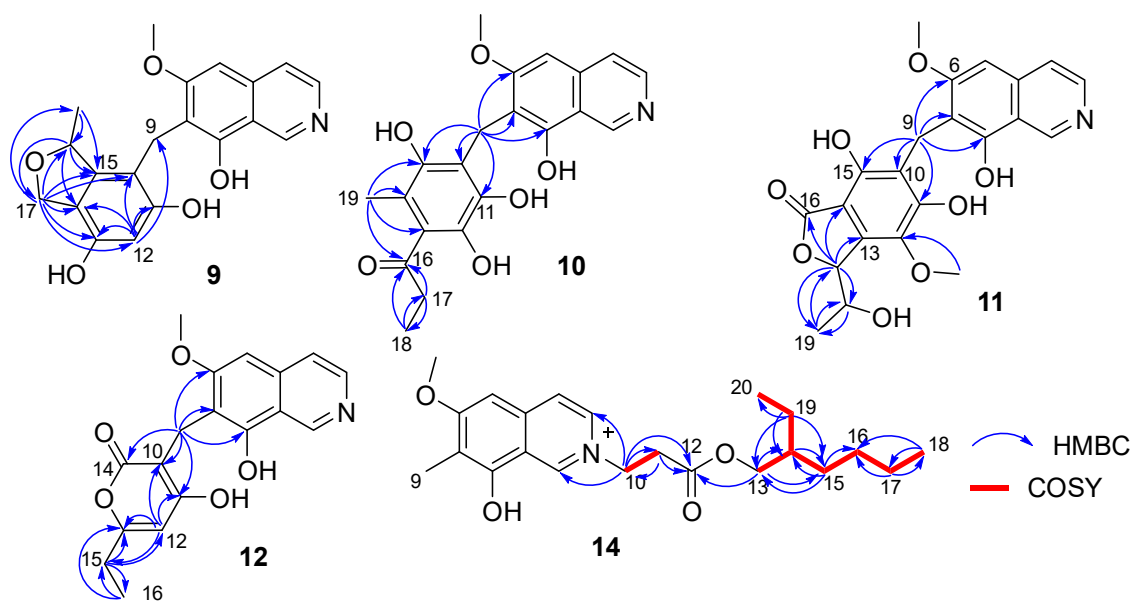
Figure 4. Key COSY and HMBC correlations of compounds **9–12** and **14**.

The calculated weighted ECD spectrum of (16R)-**9** agreed well with the experimental ECD spectrum of **9** (Figure 5), leading to the assignment of the absolute configuration at C-16.
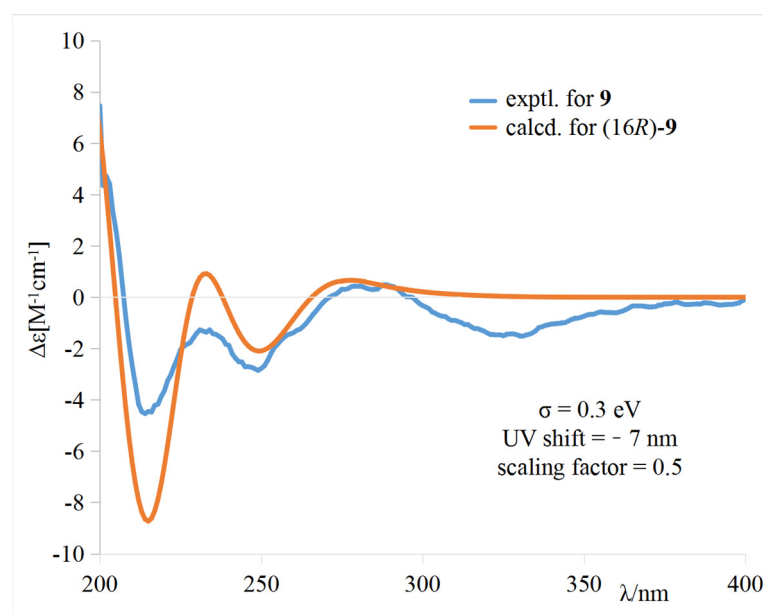
Figure 5. Comparison of the experimental and calculated ECD spectra of **9** in CH_3OH.

Puniceusine J (**10**) had the molecular formula of $C_{21}H_{21}NO_6$, as determined by its HRESIMS. The ^1H and ^{13}C NMR data of **10** (Tables 3 and 4) were very similar to those of **8** and **9**. A detailed analysis of HSQC and HMBC spectra proved that **10** also contained a benzyl attached at position C-7 of isoquinoline unit. The HMBC correlations of H_2-9 with C-6/C-7/C-8/C-10/C-11 (δ_C 170.0, C)/C-15 (δ_C 171.6, C) (Figure 4) suggested two hydroxyl groups attached at C-11 and C-15, respectively. In addition, the HMBC correlations from H_3-19 (δ_H 1.92, 3H, s) to C-13/C-14/C-15 suggested a methyl attached at C-14. Furthermore, the HMBC correlations (Figure 4) from H_2-17 (δ_H 2.58, 2H, q, *J* = 7.3 Hz) to C-16/C-18, from H_3-18 (δ_H 1.02, 3H, t, *J* = 7.3 Hz) to C-16/C-17, and from H_3-19 to C-16 suggested an 1-acetonyl group attached at C-13. Lastly, the chemical shift of C-12 (δ_C 163.1, C) indicated a hydroxy group attached at C-12. Therefore, the structure of **10** was established as shown.

Puniceusine K (**11**) was found to have the molecular formula $C_{22}H_{21}NO_8$ by HRESIMS. The ^1H and ^{13}C NMR data of **11** (Tables 3 and 4) were very similar to those of **10**. A detailed analysis of HSQC and HMBC spectra proved that **11** also contained a hexasubstituted benzyl attached at position C-7 of isoquinoline unit. The HMBC correlations of H_2-9 with C-6/C-7/C-8/C-10/C-11 (δ_C 157.1, C)/C-15 (δ_C 153.0, C) suggested two hydroxyl groups attached at C-11 and C-15, respectively. Additionally, the HMBC correlations (Figure 4) from H-17 (δ_H 5.56, d, *J* = 2.5 Hz) to C-13/C-14/C-16/C-18/C-19, from H-18 (δ_H 4.36, qd, *J* = 6.5, 2.5 Hz) to C-19, and from H_3-19 (δ_H 0.94, d, *J* = 6.5 Hz, 3H) to C-17/C-18, suggested a 5-hydroxy-2-hexene-4-lactone group attached on the benzene ring via C-13 and C-14. In addition, the HMBC correlation of δ_H 3.76 (s, 3H) with C-12 (δ_C 136.8, C) suggested a methoxy group attached at C-12 of the benzene ring. The assignment of the substituent groups at positions C-12, C-13 and C-14 of the benzene ring was further supported by comparison of the ^1H and ^{13}C NMR data of the same isobenzofuran moiety in **11**, embeurekol C [17] and acetophthalidin [18]. In addition, the small $^3J_{HH}$ value (2.5 Hz) between H-17 and H-18 in **11** was closely similar to that of embeurekol C [17]. Furthermore, the specific rotation value of **11** ($[\alpha]_D^{25}$ −9.1 (*c* 0.1, CH_3OH)) was close to that of embeurekol C ($[\alpha]_D^{20}$ −17 (*c* 0.05, CH_3OH)) [17], and the experimental ECD spectrum of **11** (Figure S76) was greatly similar to that of embeurekol C [17]. These data suggested that the absolute configuration of **11** was also 17*R*, 18*S* for that of embeurekol C.

Puniceusine L (**12**) had a molecular formula of $C_{18}H_{17}NO_5$ on the basis of its HRESIMS and NMR data. Its ^1H and ^{13}C NMR data (Tables 3 and 4) showed a similarity to those of **8–11**. A detailed analysis of HSQC and HMBC spectra suggested that **12** contained the same isoquinoline unit as **8–11**. In addition, considering the molecular formula and unsaturation degrees of **12**, the HMBC correlations from H_2-9 to C-6/C-7/C-8/C-10/C-11/C-14, from H-12 to C-10/C-11/C-13/C-15, from H_2-15 to C-12/C-13/C-16, and from H_3-16 to C-13/C-15 (Figure 4), suggested a 6-ethyl-4-hydroxy-2*H*-pyran-2-one unit attached at the methylene C-9 of isoquinoline unit. The above assignment was further confirmed by a single crystal X-ray diffraction analysis (Figure 3).

Puniceusine M (**13**) had the molecular formula of $C_{19}H_{19}NO_5$ on the basis of its HRESIMS. The ^1H and ^{13}C NMR data (Tables 3 and 4) were very similar to those of **12**. The only difference between them was the disappearance of one aromatic hydrogen and the additional presence of a methyl (δ_H 2.01 (3H, s), δ_C 9.9). The HMBC correlations from H_3-17 (δ_H 2.01) to C-11/C-12/C-13 suggested the additional methyl attached at C-12. Therefore, the structure of **13** was established as shown.

Puniceusine N (**14**) had the molecular formula $C_{22}H_{32}NO_4^+$, as determined by HRES-IMS. The ^1H and ^{13}C NMR (Tables 3 and 4) data of **14** showed a similarity to those of **2**, and the clearest difference between them was the additional presence of two methyls, seven methylenes (one oxygenated), one methine, and one carboxyl in **14**. Detailed analysis of the HMBC and COSY spectra proved that **14** contained the same isoquinoline unit as that of **2**. In addition, combining with the COSY correlation of H_2-10 (δ_H 4.88, t, *J* = 6.3 Hz) with H_2-11 (δ_H 3.18, t, *J* = 6.3 Hz) (Figure 4), the HMBC correlations from H_2-10 to C-1/C-3/C-11/C-12 (δ_C 171.8, C), and from H_2-11 to C-9/C-12 (Figure 4), suggested a -CH_2-CH_2-COO- group attached at the nitrogen atom of isoquinoline unit. Furthermore, the sequential COSY correlations of H_2-13/H-14/H_2-15/H_2-16/H_2-17/H_2-18, and H-14/H_2-19/H_3-20 (Figure 4), together with the HMBC correlations from H_2-13 to C-12/C-14/C-15, from H_2-15 to C-13/C-14/C-16, from H_2-17 to C-16/C-18, from H_3-18 to C-16/C-17, from H_2-19 to C-13/C-14/C-15/C-20, and from H_3-20 to C-14/C-19 (Figure 4), suggested that the 2-ethylhexanol group connected with the carboxyl of the -CH_2-CH_2-COO- group to form an ester. The optical rotation and measured CD data of **14** were zero, which indicated **14** was a racemic mixture. However, an HPLC analysis of **14** with a chiral column (CHIRALPAK IA and IB, respectively, 4.6 mm × 250 mm column), eluting with n-hexane/ethanol/TFA (Figures S99 and S100), showed a big trailing peak. The reason for this could be that the two kinds of chiral columns were not suitable for the chiral separation of **14**. Thus, the structure of **14** was determined as shown.

All of the 14 compounds were evaluated for their enzyme inhibitory activity against five PTPs including CD45, SHP1, TCPTP, PTP1B and LAR, cytotoxicity towards human lung adenocarcinoma cell line H1975, and antibacterial activity. The results of protein phosphatase inhibition assays (Table 5) showed that only **3** and **4** selectively exhibited significant inhibitory activity against CD45 with IC_{50} values of 8.4 and 5.6 µM, respectively, and **1**, **8**, **9**, **10**, **12** and **13** showed a mild inhibitory activity against several PTPs. A cytotoxicity assay (Table 5) showed that only **4** had a moderate cytotoxicity towards H1975 cell lines with an IC_{50} value of 11.0 µM. The analysis of the relationship of their structures, enzyme inhibitory activity and cytotoxicity displayed that the substituents at C-7 of the isoquinoline nucleus could greatly affect their bioactivity. In addition, antibacterial assays exhibited that **14** had medium antibacterial activity towards *Staphylococcus aureus*, methicillin-resistant *S. aureus* (MRSA), and *Escherichia coli*, with MIC values of 100 µg/mL, and **4** could inhibit the growth of *E. coli* with a MIC value of 100 µg/mL, while other compounds did not show clear antibacterial activity towards the three indicators. The results indicated that -C=N^+ unit was an active center for the antibacterial activity of **14**.

Table 5. Inhibition activity against five phosphatases and cytotoxicity of **1**–**14**.

Comp.	Inhibitory Effect against Phosphatases (IC$_{50}$ in μM)					Cytotoxicity (IC$_{50}$ in μM)
	CD45	**SHP1**	**TCPTP**	**PTP1B**	**LAR**	**H1975 Cell (after 24 h)**
1	29.7	38.3	196.9	182.2	100	76.2
2	>200	>200	>200	>200	>200	>80
3	8.4	20.7	>200	64.5	21.9	71.3
4	5.6	130.2	>200	150	26.1	11.0
5	102.6	145.1	>200	200	>200	>80
6	>200	200	>200	>200	>200	>80
7	>200	>200	>200	>200	>200	>80
8	49.0	100	>200	180	>200	>80
9	27.2	41.8	57.7	68.8	>200	>80
10	30.8	>200	>200	>200	100	>80
11	100	145.4	>200	190	>200	>80
12	38.5	116.8	>200	170	150	>80
13	11.1	40.26	>200	37.9	32.6	>80
14	200	>200	>200	>200	>200	>80
Na$_3$VO$_4$	-	4.4	2.4	1.6	-	-
AACQ	0.29	-	-	-	-	-

AACQ: (2-[(4-acetylphenyl)amino]-3-chloronaphthoquinone); "-": Not tested.

3. Experimental Section

3.1. General Experimental Procedure

The procedures were the same as previously reported [13,14].

3.2. Fungal Material

The strain *Aspergillus puniceus* SCSIO z021 was isolated from a deep-sea sediment of Okinawa Trough (27°34.01′ N and 126°55.59′ E, ~1589 depth), which was located approximately 4.7 km from an active hydrothermal vent. The strain (GenBank accession number KX258801) was identified as *Aspergillus puniceus* through DNA extraction, ITS sequence amplification and sequence alignment, which has a 99% similarity to *A. puniceus* (GenBank accession number GU456970). The strain *A. puniceus* SCSIO z021 was deposited in the RNAM Center, South China Sea Institute of Oceanology, Chinese Academy of Science.

3.3. Fermentation and Extraction

The fungus strain was cultivated on potato glucose agar (PDA) plate containing 3% sea salt at 28 °C for 7 days. The spores were selected and transferred to a complex culture medium (glucose 1%, D-mannitol 2%, maltose 2%, corn meal 0.05%, monosodium glutamate 1%, KH$_2$PO$_4$ 0.05%, MgSO$_4$·7H$_2$O 0.03%, yeast extract 0.3%, sea salt 3%) to obtain a spore suspension that was cultured in a shaker at 28 °C for 3 days at a rotating speed of 180 rmp. The fungus was cultured in 1 L Erlenmeyer flasks each containing 300 mL of 3# medium (glucose 1%, D-mannitol 2%, maltose 2%, corn meal 0.05%, monosodium glutamate 1%, KH$_2$PO$_4$ 0.05%, MgSO$_4$·7H$_2$O 0.03%, yeast extract 0.3%, sea salt 3%) at 28 °C for 33 days under static condition. After fermentation, the broth and mycelia were separated with gauze. The broth was extracted with XAD-16 resin and sequentially eluted with H$_2$O and EtOH to obtain crude extract (61.7 g). The mycelia was extracted three times with acetone, and further extracted three times with EtOAc to yield a crude extract (48.2 g).

3.4. Isolation and Purification

The combined extracts (109.9 g) were subjected to a normal-phase silica gel column eluting with a gradient of dichloromethane (DCM)/MeOH (100:0, 98:2, 95:5, 95:5, 90:10, 80:20, 70:30, 50:50, 0:100) to give nine subfractions (Fr.1–Fr.9) based on TLC analysis. Fr.4 (6.6 g) was separated by ODS column using MeOH-H$_2$O-TFA (5:95:0.02 to 100:0:0.02) as eluent to afford 10 subfractions (Fr.4.1–Fr.4.10). Fr.4.1 was separated by Sephadex LH-20 eluting with MeOH followed by semipreparative HPLC (MeOH/H$_2$O/TFA, 28:72:0.03,

3 mL/min) to yield **1** (11.6 mg, t_R = 15.8 min). Fr.4.3 was subjected to Sephadex LH-20 using MeOH as mobile phase, which was further purified by semipreparative HPLC (CH₃CN/H₂O/TFA, 17:83:0.03, 3 mL/min) to yield **2** (30.7 mg, t_R = 16.3 min). Fr.4.5 was isolated by Sephadex LH-20 eluting with MeOH, then purified by semipreparative HPLC (CH₃CN/H₂O/TFA, 25:75:0.03, 3 mL/min) to yield **7** (2.9 mg, t_R = 25.9 min). Fr.4.6 was separated by Sephadex LH-20 with a mobile phase of MeOH, and then further purified by semipreparative HPLC (MeOH/H₂O/TFA, 45:55:0.03, 3 mL/min) to yield **10** (2.8 mg, t_R = 16.1 min) and **12** (15.2 mg, t_R = 14.5 min). Fr.4.8 was isolated by silica gel column eluting with a gradient of CH₂Cl₂/MeOH (100:0, 80:1, 60:1, 40:1, 10:1, 5:1, 1:1, 0:100) to obtain three fractions, then Fr.4.8.1 was further purified by semipreparative HPLC (CH₃CN/H₂O/TFA, 49:51:0.03, 3 mL/min) to yield **14** (29.4 mg, t_R = 20.2 min). Fr.6 (11.0 g) was separated by ODS column using MeOH-H₂O-TFA (5:95:0.02 to 100:0:0.02) as mobile phase to yield eight subfractions (Fr.6.1–Fr.6.8). Fr.6.3 was purified by semipreparative HPLC (CH₃CN/H₂O/TFA, 21:79:0.03, 3 mL/min) to obtain **6** (4.0 mg, t_R = 19.5 min), **3** (17.6 mg, t_R = 18.4 min) and **4** (12.2 mg, t_R = 19.7 min). Fr.6.6 was isolated by semipreparative HPLC (CH₃CN/H₂O/TFA, 24:76:0.03, 3 mL/min) to yield **11** (7.8 mg, t_R = 16.0 min) and **5** (4.3 mg, t_R = 14.4 min). Fr.6.7 was isolated by Sephadex LH-20 with MeOH as mobile phase, then further purified by semipreparative HPLC (CH₃CN/H₂O/TFA, 28:72:0.03, 3 mL/min) to yield **8** (4.1 mg, t_R = 39.2 min) and **9** (2.8 mg, t_R = 18.4 min). Fr.6.8 was separated by Sephadex LH-20, eluting with MeOH and further purified by semipreparative HPLC (CH₃CN/H₂O/TFA, 35:65:0.03, 3 mL/min) to get **13** (10.3 mg, t_R = 18.0 min).

Puniceusine A (**1**): white acicular crystal; UV (CH₃OH) λ_{max} (log ε) 204 (1.42), 208 (1.42), 241 (1.56), 258 (1.58), 357 (0.74) nm; ¹H and ¹³C NMR, Tables 1 and 2; HRESIMS m/z 176.0709 [M + H]⁺ (calcd for $C_{10}H_{10}NO_2$, 176.0706).

Puniceusine B (**2**): pale yellow powder; UV (CH₃OH) λ_{max} (log ε) 206 (1.61), 245 (1.75), 260 (1.83), 305 (0.73), 360 (0.84) nm; ¹H and ¹³C NMR, Tables 1 and 2; HRESIMS m/z 190.0864 [M + H]⁺ (calcd for $C_{11}H_{12}NO_2$, 190.0863).

Puniceusine C (**3**): pale yellow powder; UV (CH₃OH) λ_{max} (log ε) 205 (1.87), 244 (1.98), 262 (2.04), 332 (1.07) nm; IR (film) ν_{max} 3415, 1678, 1436, 1382, 1321, 1203, 1184, 1130, 1022, 954, 900, 840, 800, 723 cm⁻¹; ¹H and ¹³C NMR, Tables 1 and 2; HRESIMS m/z 363.1339 [M + H]⁺ (calcd for $C_{21}H_{19}N_2O_4$, 363.1349).

Puniceusine D (**4**): pale yellow powder; UV (CH₃OH) λ_{max} (log ε) 207 (1.86), 243 (1.88), 260 (1.88) nm; IR (film) ν_{max} 3402, 1678, 1643, 1566, 1384, 1342, 1197, 1132, 1045, 989, 954, 842, 800, 723 cm⁻¹; ¹H and ¹³C NMR, Tables 1 and 2; HRESIMS m/z 363.1339 [M + H]⁺ (calcd for $C_{21}H_{19}N_2O_4$, 363.1338).

Puniceusine E (**5**): pale yellow powder; UV (CH₃OH) λ_{max} (log ε) 206 (2.07), 248 (1.83), 265 (2.00), 337 (1.06) nm; IR (film) ν_{max} 1703, 1678, 1365, 1178, 0012, 835, 800, 721 cm⁻¹; ¹H and ¹³C NMR, Tables 1 and 2; HRESIMS m/z 377.1496 [M + H]⁺ (calcd for $C_{22}H_{21}N_2O_4$, 377.1486).

Puniceusine F (**6**): colorless crystals; $[\alpha]_D^{25}$ 0 (*c* 0.10, CH₃OH); UV (CH₃OH) λ_{max} (log ε) 206 (1.63), 244 (1.76), 261 (1.71) nm; IR (film) ν_{max} 3419, 1703, 1681, 1363, 1201, 1180, 1134, 837, 800, 721 cm⁻¹; ¹H and ¹³C NMR, Tables 1 and 2; HRESIMS m/z 262.1076 [M + H]⁺ (calcd for $C_{14}H_{16}NO_4$, 262.1074).

Puniceusine G (**7**): yellow powder; UV (CH₃OH) λ_{max} (log ε) 200 (1.26), 246 (1.46) nm; IR (film) ν_{max} 3412, 1680, 1440, 1195, 1136, 1028, 844, 800, 725 cm⁻¹; ¹H and ¹³C NMR, Tables 1 and 2; HRESIMS m/z 254.1182 [M + H]⁺ (calcd for $C_{16}H_{16}NO_2$, 254.1176).

Puniceusine H (**8**): pale yellow powder; UV (CH₃OH) λ_{max} (log ε) 191 (1.61), 204 (2.08), 242 (1.06), 272 (1.12) nm; IR (film) ν_{max} 3367, 1680, 1456, 1417, 1394, 1201, 1139, 1020, 839, 802, 721 cm⁻¹; ¹H and ¹³C NMR, Tables 2 and 3; HRESIMS m/z 398.1244 [M + H]⁺ (calcd for $C_{21}H_{20}NO_7$, 398.1234).

Puniceusine I (**9**): yellow powder; $[\alpha]_D^{25}$ + 60.7 (*c* 0.10, CH₃OH); UV (CH₃OH) λ_{max} (log ε) 205 (1.30), 237 (0.90), 244 (0.92), 276 (0.63) nm; ECD (CH₃OH) λ_{max} ($\Delta\varepsilon$) 201 (+4.35), 202 (+4.71), 214 (−4.54), 232 (−1.32), 246 (−2.71), 279 (+0.44), 322 (−1.45) nm; IR (film) ν_{max}

3402, 1699, 1681, 1361, 1201, 1136, 837, 800, 721 cm^{-1}; ^{1}H and ^{13}C NMR, Tables 3 and 4; HRESIMS m/z 354.1331 [M + H]$^+$ (calcd for C$_{20}$H$_{20}$NO$_5$, 354.1336).

Puniceusine J (**10**): pale yellow powder; UV (CH$_3$OH) λ_{max} (log ε) 195 (2.08), 208 (1.06), 243 (1.12) nm; IR (film) ν_{max} 3406, 1678, 1392, 1321, 1203, 1132, 840, 800, 723 cm^{-1}; ^{1}H and ^{13}C NMR, Tables 3 and 4; HRESIMS m/z 384.1455 [M + H]$^+$ (calcd for C$_{21}$H$_{22}$NO$_6$, 384.1442).

Puniceusine K (**11**): pale yellow powder; $[\alpha]_D^{25}$ − 155.6 (*c* 0.10, CH$_3$OH); UV (CH$_3$OH) λ_{max} (log ε) 205 (1.30), 237 (0.90), 244 (0.92), 276 (0.63) nm; ECD (CH$_3$OH) λ_{max} ($\Delta\varepsilon$) 215 (−2.39), 229 (+0.45), 238 (+0.29), 255 (+0.67), 304 (−0.18) nm; IR (film) ν_{max} 3390, 1674, 1435, 1371, 1319, 1199, 1134, 840, 800, 723 cm^{-1}; ^{1}H and ^{13}C NMR, Tables 3 and 4; HRESIMS m/z 428.1348 [M + H]$^+$ (calcd for C$_{22}$H$_{22}$NO$_8$, 428.1340).

Puniceusine L (**12**): colorless crystals; UV (CH$_3$OH) λ_{max} (log ε) 206 (2.14), 264 (2.04), 366 (1.12) nm; IR (film) ν_{max} 3080, 1678, 1643, 1396, 1319, 1197, 1130, 839, 798, 721 cm^{-1}; ^{1}H and ^{13}C NMR, Tables 3 and 4; HRESIMS m/z 328.1195 [M + H]$^+$ (calcd for C$_{18}$H$_{18}$NO$_5$, 328.1179).

Puniceusine M (**13**): pale yellow powder; UV (CH$_3$OH) λ_{max} (log ε) 207 (2.08), 244 (1.74), 267 (1.84) nm; IR (film) ν_{max} 3404, 1678, 1394, 1319, 1201, 1176, 1138, 1026, 837, 800, 721 cm^{-1}; ^{1}H and ^{13}C NMR, Tables 3 and 4; HRESIMS m/z 342.1332 [M + H]$^+$ (calcd for C$_{19}$H$_{20}$NO$_5$, 342.1336).

Puniceusine N (**14**): pale yellow powder; $[\alpha]_D^{25}$ 0 (*c* 0.10, CH$_3$OH); UV (CH$_3$OH) λ_{max} (log ε) 206 (1.89), 232 (1.61), 266 (2.08), 309 (1.06), 364 (1.12) nm; IR (film) ν_{max} 3423, 1680, 1363, 1195, 1182, 1128, 839, 800, 719 cm^{-1}; ^{1}H and ^{13}C NMR, Tables 3 and 4; HRESIMS m/z 374.2329 [M]$^+$ (calcd for C$_{22}$H$_{32}$NO$_4$, 374.2326).

3.5. X-ray Crystallographic Analysis of **6** and **12**

The crystal data were obtained on a Rigaku MicroMax 007 diffractometer (Rigaku Corporation, Tokyo, Japan)with Cu Kα radiation and a graphite monochromator. The crystal structures of **6** and **12** were solved by direct methods with the SHELXTL and refined by full-matrix, least-squares techniques. Crystallographic data for **6** and **12** were deposited with the Cambridge Crystallographic Data Centre as supplementary publication numbers, CCDC 2112471 and 2112479, respectively.

Crystal data for **6**: C$_{14}$H$_{14.0375}$NO$_4$, *FW* = 260.30; colorless crystal from MeOH; crystal size = 0.15 × 0.12 × 0.1 mm^3; *T* = 100.00 (10) K; monoclinic, space group P2$_1$/c (no. 14); unit cell parameters: *a* = 4.82780 (10) Å, *b* = 13.4963 (3) Å, *c* = 22.6665 (7) Å, α = 90°, β = 96.025 (3)°, γ = 90°, *V* = 1468.73 (6) Å^3, *Z* = 4, *D*$_{calc}$ = 1.177 g/cm^3, *F* (000) = 548.0, μ (CuKα) = 0.724 mm^{-1}; 7185 reflections measured (7.634° $\leq$ 2θ $\leq$ 147.79°), 2852 unique (*R*$_{int}$ = 0.0197, R$_{sigma}$ = 0.0255), which were used in all calculations. The final R$_1$ was 0.0487 (I > 2σ(I)) and *w*R$_2$ was 0.1406 (all data).

Crystal data for **12**: C$_{18}$H$_{17}$NO$_5$, *FW* = 327.32; colorless crystal from MeOH; crystal size = 0.13 × 0.12 × 0.1 mm^3; *T* = 100.00 (10) K; triclinic, space group P-1 (no. 2); unit cell parameters: *a* = 7.6037 (4) Å, *b* = 9.9253 (5) Å, *c* = 10.5261 (6) Å, α = 70.543 (5)°, β = 85.628 (4)°, γ = 81.605 (4)°, *V* = 740.68(7) Å^3, *Z* = 2, *D*$_{calc}$ = 1.468 g/cm^3, *F* (000) = 344.0, μ (CuKα) = 0.897 mm^{-1}; 7019 reflections measured (8.914° $\leq$ 2θ $\leq$ 148.202°), 2880 unique (*R*$_{int}$ = 0.0259, R$_{sigma}$ = 0.0317) which were used in all calculations. The final R$_1$ was 0.0419 (I > 2σ(I)) and *w*R$_2$ was 0.1150 (all data).

3.6. ECD Calculations

The ECD calculation for **9** was performed by Gaussian 16 program package. The procedures were the same as described in our previous study [13,14]. Briefly, the conformational search was performed by a MMFF model, then the conformers with lower relative energies (<10 kcal/mol) were subjected to geometry optimization with the DFT method at the B3LYP/6-311G(d) level. Vibrational frequency calculations were carried out at the same level to evaluate their relative thermal (ΔE) and free energies (ΔG) at 298.15 K. The geometry-optimized conformers were further calculated at the M06-2X/def2-TZVP level and the

solvent (methanol) effects were taken into consideration by using SMD. The optimized conformers with a Boltzmann distribution of more than 1% population were subjected to ECD calculation, which were performed by TDDFT methodology at the PBE1PBE/TZVP level. The ECD spectrum was generated by the software SpecDis using a Gaussian band shape with 0.3 eV exponential half-width from dipole-length dipolar and ratational strengths. The calculated spectrum of **9** was generated from the low-energy conformers according to the Boltzmann distribution of each conformer in MeOH solution. Details regarding optimized conformation geometries, thermodynamic parameters, and Boltzmann distributions (Tables S1–S3) of all conformations are provided in the Supporting Information.

3.7. Protein Phosphatase Inhibition Assays

The same methods as described in our previous study [13,14] were applied to test the inhibition activity of compounds **1**–**14** against five human protein tyrosine phosphatases (CD45, SHP1, TCPTP, PTP1B and LAR).

3.8. Cytotoxicity

Cytotoxic activity was evaluated using human lung adenocarcinoma cell line H1975 by CCK-8 method. Briefly, each of the test compounds was dissolved in DMSO and further diluted to give final concentrations of 80, 40, 20, 10, 5, 2.5, and 1.25 μg/mL, respectively. H1975 cells (5×10^3 cells/plate) were seeded in 96-well plates and treated with compounds at the indicated concentration for 24 h, and then 10 μL CCK-8 reagent was added to each well, and the plates were incubated at 37 °C for another 4 h. Next, the optical density was measured at a wavelength of 450 nm with the Bio-Rad (Hercules, CA, USA) microplate reader. Dose–response curves were generated, and the IC_{50} values were calculated from the linear portion of log dose–response curves.

3.9. Antibacterial Assays

Antibacterial activities of **1**–**14** against *E. coli*, *S. aureus* and MRSA were evaluated using the 2-fold dilution assay in 96-microwell plates. Briefly, all the indicator bacteria were cultured on Luria−Bertani (LB) agar plates at 37 °C for 12 h, and then a single colony was picked into LB liquid medium and cultivated on a rotary shaker at 37 °C for 12 h. Then, the bacterial suspensions with LB medium were diluted until the difference of the OD_{600} values between the bacterial suspensions and the medium was 0.01~0.02. Each of the tested compounds was dissolved in DMSO to give an initial concentration of 5 mg/mL, and further diluted with the bacterial suspensions by twofold serial dilution to give a final concentration of 100, 50, 25, 12.5, 6.25, and 3.125 μg/mL, respectively. The 96-well plates were incubated at 37 °C for 12 h. MIC value was determined as the lowest concentration with no visible bacterial growth. Ampicillin was used as the positive control and DMSO as the negative control. All experiments were performed three times.

4. Conclusions

Summarily, 14 new isoquinoline alkaloids (**1**–**14**) were obtained from the deep-sea-derived fungus, *A. puniceus* SCSIO z021. Compounds **3**–**5** and **8**–**13** unprecedentedly contained an isoquinolinyl, a polysubstituted benzyl or a pyronyl at position C-7 of the isoquinoline nucleus, which was different from 1-benzylisoquinoline analogues and other isoquinoline alkaloids from plants commonly containing substituents at positions C-1, N-2, C-3, C-4 or C-8 of isoquinoline skeleton. In addition, **3** and **4** showed selective inhibitory activity against CD45; **4** also had moderate cytotoxicity towards human lung adenocarcinoma cell line H1975, and **14** contained an active center -C=N$^+$ which had evident antibacterial activity towards three indicator bacteria. An analysis of the relationship of the structures, enzyme inhibitory activity and cytotoxicity of **1**–**14** displayed that the substituents at C-7 of the isoquinoline nucleus could greatly affect their bioactivity. The results greatly enrich the structural diversity of isoquinoline alkaloids from fungi, and provide a potential lead compound for the development of a selective CD45 inhibitor and anticancer drug.

References

1. Singh, S.; Pathak, N.; Fatima, E.; Negi, A.S. Plant isoquinoline alkaloids: Advances in the chemistry and biology of berberine. *Eur. J. Med. Chem.* **2021**, *226*, 113839. [CrossRef] [PubMed]

2. Kohno, J.; Hiramatsu, H.; Nishio, M.; Sakurai, M.; Okuda, T.; Komatsubara, S. Structures of TMC-120A, B and C, novel isoquinoline alkaloids from *Aspergillus ustus* TC 1118. *Tetrahedron* **1999**, *55*, 11247–11252. [CrossRef]

3. Copmans, D.; Kildgaard, S.; Rasmussen, S.A.; Ślezak, M.; Dirkx, N.; Partoens, M.; Esguerra, C.V.; Crawford, A.D.; Larsen, T.O.; de Witte, P.A.M. Zebrafish-based discovery of antiseizure compounds from the North Sea: Isoquinoline alkaloids TMC-120A and TMC-120B. *Mar. Drugs* **2019**, *17*, 607. [CrossRef] [PubMed]

4. Li, G.Y.; Li, B.G.; Yang, T.; Liu, G.Y.; Zhang, G.L. Chaetoindicins A-C, three isoquinoline alkaloids from the fungus *Chaetomium indicum*. *Org. Lett.* **2006**, *8*, 3613–3615. [CrossRef] [PubMed]

5. Yang, S.X.; Xiao, J.; Laatsch, H.; Holstein, J.J.; Dittrich, B.; Zhang, Q.; Gao, J.M. Fusarimine, a novel polyketide isoquinoline alkaloid, from the endophytic fungus *Fusarium* sp. ln12, isolated from *Melia azedarach*. *Tetrahedron Lett.* **2012**, *53*, 6372–6375. [CrossRef]

6. El-Neketi, M.; Ebrahim, W.; Lin, W.; Gedara, S.; Badria, F.; Saad, H.E.; Lai, D.; Proksch, P. Alkaloids and polyketides from *Penicillium citrinum*, an endophyte isolated from the Moroccan plant *Ceratonia siliqua*. *J. Nat. Prod.* **2013**, *76*, 1099–1104. [CrossRef] [PubMed]

7. Yang, W.C.; Yuan, J.; Tan, Q.; Chen, Y.; Zhu, Y.J.; Jiang, H.M.; Zou, G.; Zang, Z.Z.; Wang, B.; She, Z.G. Peniazaphilones A–I, produced by co-culturing of mangrove endophytic fungi, *Penicillium sclerotiorum* THSH-4 and *Penicillium sclerotiorum* ZJHJJ-18. *Chin. J. Chem.* **2021**, *39*, 3404–3412. [CrossRef]

8. Nord, C.; Levenfors, J.J.; Bjerketorp, J.; Sahlberg, C.; Guss, B.; Öberg, B.; Broberg, A. Antibacterial isoquinoline alkaloids from the fungus *Penicillium spathulatum* Em19. *Molecules* **2019**, *24*, 4616. [CrossRef] [PubMed]

9. Bialy, L.; Waldmann, H. Inhibitors of protein tyrosine phosphatases: Next-generation drugs? *Angew. Chem. Int. Ed. Engl.* **2005**, *44*, 3814–3839. [CrossRef] [PubMed]

10. Barr, A.J. Protein tyrosine phosphatases as drug targets: Strategies and challenges of inhibitor development. *Future Med. Chem.* **2010**, *2*, 1563–1576. [CrossRef] [PubMed]

11. Pan, D.Y.; Zhang, X.X.; Zheng, H.Z.; Zheng, Z.H.; Nong, X.H.; Liang, X.; Ma, X.; Qi, S.H. Novel anthraquinone derivatives as inhibitors of protein tyrosine phosphatases and indoleamine 2,3-dioxygenase 1 from the deep-sea derived fungus *Alternaria tenuissima* DFFSCS013. *Org. Chem. Front.* **2019**, *6*, 3252–3258. [CrossRef]

12. Cheng, X.; Liang, X.; Zheng, Z.H.; Zhang, X.X.; Lu, X.H.; Yao, F.H.; Qi, S.H. Penicimeroterpenoids A–C, meroterpenoids with rearrangement skeletons from the marine-derived fungus *Penicillium* sp. SCSIO 41512. *Org. Lett.* **2020**, *16*, 6330–6333. [CrossRef] [PubMed]

13. Liang, X.; Huang, Z.H.; Ma, X.; Zheng, Z.H.; Zhang, X.X.; Lu, X.H.; Qi, S.H. Mycotoxins as inhibitors of protein tyrosine phosphatases from the deep-sea-derived fungus *Aspergillus puniceus* SCSIO z021. *Bioorg. Chem.* **2021**, *107*, 104571. [CrossRef] [PubMed]

14. Liang, X.; Huang, Z.H.; Shen, W.B.; Lu, X.H.; Zhang, X.X.; Ma, X.; Qi, S.H. Talaromyoxaones A and B: Unusual oxaphenalenone spirolactones as phosphatase inhibitors from the marine-derived fungus *Talaromyces purpureogenus* SCSIO 41517. *J. Org. Chem.* **2021**, *86*, 12831–12839. [CrossRef] [PubMed]

15. White, J.D.; Straus, D.S. Gattermann reaction of 3,5-dimethoxyphenylacetonitrile. Synthesis of 6,8-dioxyisoquinolines. *J. Org. Chem.* **2002**, *32*, 2689–2692. [CrossRef]

16. Atta-ur-Rahman; Ahmad, S.; Bhatti, M.K.; Choudhary, M.I. Alkaloidal constituents of *Fumaria indica*. *Phytochemistry* **1995**, *40*, 593–596. [CrossRef]

17. Ebrahim, W.; Aly, A.H.; Mándi, A.; Wray, V.; Essassi, E.; Ouchbani, T.; Bouhfid, R.; Lin, W.; Proksch, P.; Kurtán, T.; et al. O-heterocyclic embeurekols from *Embellisia eureka*, an endophyte of *Cladanthus arabicus*. *Chirality* **2013**, *25*, 250–256. [CrossRef] [PubMed]

18. Cui, C.B.; Ubukata, M.; Kakeya, H.; Onose, R.; Okada, G.; Takahashi, I.; Isono, K.; Osada, H. Acetophthalidin, a novel inhibitor of mammalian cell cycle, produced by a fungus isolated from a sea sediment. *J. Antibiot.* **1996**, *49*, 216–219. [CrossRef] [PubMed]